

Published in final edited form as:

*Nat Cell Biol.* 2015 November ; 17(11): 1412–1421. doi:10.1038/ncb3250.

## Integrin endosomal signalling suppresses anoikis

Jonna Alanko<sup>1,2</sup>, Anja Mai<sup>1</sup>, Guillaume Jacquemet<sup>1</sup>, Kristine Schauer<sup>3</sup>, Riina Kaukonen<sup>1</sup>, Markku Saari<sup>1,2</sup>, Bruno Goud<sup>3</sup>, and Johanna Ivaska<sup>1,2,4</sup>

<sup>1</sup>Turku Centre for Biotechnology, University of Turku, Turku, Finland <sup>2</sup>VTT Technical Research Centre of Finland, Turku, Finland <sup>3</sup>Molecular Mechanisms of Intracellular Transport, Institut Curie, Paris, France <sup>4</sup>Department of Biochemistry and Food Chemistry, University of Turku, FIN-20520, Finland

### Abstract

Integrin containing focal adhesions (FAs) transmit extracellular signals across the plasma membrane to modulate cell adhesion, signalling and survival. Although integrins are known to undergo continuous endo/exocytic traffic, potential impact of endocytic traffic on integrin-induced signals is unknown. Here, we demonstrate that integrin signalling is not restricted to cell-ECM adhesions and identify an endosomal signalling platform that supports integrin signalling away from the plasma membrane. We show that active focal adhesion kinase (FAK), an established marker of integrin-ECM downstream signalling, localises with active integrins on endosomes. Integrin endocytosis positively regulates adhesion-induced FAK activation, which is early endosome antigen-1 (EEA1) and small GTPase Rab21 dependent. FAK binds directly to purified endosomes and becomes activated on them, suggesting a role for endocytosis in enhancing distinct integrin downstream signalling events. Finally, endosomal integrin signalling contributes to cancer-related processes such as anoikis resistance, anchorage-independence and metastasis.

Integrins are heterodimeric cell surface adhesion receptors functioning as integrators of the extracellular matrix (ECM) driven cues, the cellular cytoskeleton and the cellular signalling apparatus 1. Upon adhesion, integrins trigger the formation of plasma-membrane proximal large mechanosensing and signal-transmitting protein clusters depicted as “adhesomes” 2, 3. In addition, integrins undergo constant endocytic traffic to facilitate focal adhesion turnover, cell migration, invasion and cytokinesis 4. For other receptor systems it is well established that endocytic membrane traffic regulates bioavailability of cell-surface molecules and therefore the intensity and/or specificity of receptor-initiated signals 5, 6. Although active integrins and their

---

Correspondence should be addressed to J.I. (johanna.ivaska@utu.fi).

#### Author Information

The mass spectrometry proteomics data have been deposited to the ProteomeXchange Consortium via the PRIDE partner repository with the dataset identifier PXD001870 and 10.6019/PXD001870.

#### Contributions

J.I. conceived and supervised the study, carried out experiments, analysed the data and wrote the manuscript with the contribution of J.A., B.G. and A.M. K.S. and B.G. supervised and helped analyse micropatterning experiments and gave helpful insights and discussion. J.A. designed, carried out and analysed most of the experiments with crucial help from A.M., R.K. and M.S. G.J. and A.M. designed, carried out and analysed the mass-spec experiments. H.H. (acknowledged) provided instrumental help in editing the manuscript text and figures.

Authors declare no conflict of interests.

ligands have been detected in endosomes 7–9 and increased integrin recycling to the plasma membrane contributes to enhanced signalling of co-trafficked receptor tyrosine kinases<sup>10, 11</sup> it has remained unclear whether endocytosed active integrins signal in endosomes. Here, we demonstrate that integrin signalling is not restricted to focal adhesions as previously described and that endocytosis is necessary for full ECM-induced, integrin mediated ERK, AKT and FAK signalling. We find that FAK binds directly to and can become activated on purified endosomes. Moreover, the FERM-domain of FAK is able to bind purified integrin containing endosomes, suggesting the potential for integrin signalling complexes to assemble on endosomes after internalization of active integrins. Importantly, FAK is required for anchorage-independent growth and suppression of anoikis<sup>12</sup>. Integrin endosomal signalling correlates with reduced anoikis sensitivity in normal cells and anchorage-independent growth and metastasis in breast cancer cells.

## Results

### Active FAK localizes to integrin-containing endosomes

Cell-ECM adhesion and activation of integrin signalling is necessary for cell survival, differentiation and developmental processes<sup>13, 14</sup>. Integrin endocytosis offers an efficient system to control integrin heterodimer availability at the cell surface and thus the specific ECM-induced cellular response during processes such as cell migration and tumour cell invasion<sup>15, 16</sup>. As FAK recruitment to focal adhesions and subsequent Y397 autophosphorylation (pFAK-Y397) is an established marker of integrin-ECM engagement and downstream signalling<sup>17</sup> we used an anti-pFAK-Y397 antibody to visualise integrin signalling and subcellular localisation in adherent cells. The pFAK-Y397 antibody detected a dominant 125 kDa protein band in wild-type FAK<sup>+/+</sup> MEFs that was absent in FAK<sup>-/-</sup> cells (Supplementary Fig. 1a) and strongly reduced upon treatment with FAK inhibitors in western blots and in immunofluorescence (Supplementary Fig. 1b, c) indicative of antibody specificity towards pFAK-Y397. Immunofluorescence analyses of cells plated on micropatterns revealed that in addition to the expected ECM-interface localization of integrin and pFAK, substantial pools of both proteins could be detected within the cell body (Supplementary Fig. 1d). Analysis of 3D probabilistic density maps<sup>18</sup> of active integrin and pFAK, in which density contours represent the smallest intracellular volume containing 50% of the total immunofluorescence signal, indicated a substantial pool of pFAK at the cell centre where it overlapped with internalised active  $\beta$ 1-integrin (9EG7 antibody) (Fig. 1a). The extent of co-localization between active  $\beta$ 1-integrin and pFAK in micropattern normalized cells (n=24) was  $38.3 \pm 6.2$  (s.d.)%, as assessed by a particle-based analysis. A similar intracellular localisation of pFAK was detected in unconstrained cells (Fig. 1b), suggesting that the non-adhesion-site-localised pFAK was not an artefact of restricting the cell geometry with micropatterns.

Exogenous expression of the constitutively active Rab5 GTPase (Rab5Q79L, Rab5-CA) results in the formation of enlarged endosome structures<sup>19</sup> and can be used to visualize endosomal localization of a variety of proteins, including integrins<sup>20</sup>. In addition, overexpression of Rab21 induces  $\beta$ 1-integrin endocytosis and localization to enlarged early endosomes<sup>9</sup>. We used these properties to further investigate the subcellular localisation of the intracellular active  $\beta$ 1-integrin and pFAK. Active  $\beta$ 1-integrin (12G10 antibody) and

pFAK were visible as closely associated puncta in both Rab5-CA and Rab21-positive endosomes in serum-starved TIFFs actively adhering to fibronectin (Fig. 1c, Rab5CA; 98.7% and Supplementary Fig. 1e, Rab21; 97.1% of active  $\beta$ 1-integrin positive endosomes contained pFAK,  $n = 243$  and 209 endosomes, respectively) and similar data were obtained using a total  $\beta$ 1-integrin antibody (Fig. 1c, Supplementary Fig. 1e). Endosomal puncta of active  $\beta$ 1-integrin and pFAK closely associated with a mean distance of  $\sim 2$ -3 pixels, a value similar to those obtained between active  $\beta$ 1-integrin and Rab5 (mean distance of  $\sim 3$  pixels; Fig 1c). Similar association between active  $\beta$ 1-integrin and pFAK was observed on EEA1- (Fig. 1b) and Rab21-positive endosomes (Supplementary Fig. 1e). For comparison, the mean distance between randomly distributed non-endosomal pFAK and pFAK (Fig. 1c and Supplementary Fig. 1e) or active  $\beta$ 1 and pFAK outside the endosomes (Fig. 1b) was  $\sim 8$ -10 pixels. These puncta co-distribution analyses indicate that active  $\beta$ 1-integrin and pFAK are found in the same endosomes. Phospho-FAK recruitment to integrin-positive endosomes was further confirmed using super resolution STED microscopy (Fig. 1d). Thus, phosphorylated FAK is not restricted to focal adhesions but can also be detected on endosomes in adherent cells.

### **Integrin ligands and talin are present in FAK-positive endosomes**

Several studies report integrin ligand localisation in endosomes 8, 10, 22 and we have demonstrated increased endosomal retention of active  $\beta$ 1-integrins compared to inactive receptors 7. Importantly, we detected the integrin ligand fibronectin in pFAK and active  $\beta$ 1-integrin-positive endosomes (Fig. 2a; 90.5% of pFAK-positive endosomes contained fibronectin,  $n = 200$  endosomes), suggesting that functional receptor-ligand coupling is linked to the endosome-associated active FAK pool. Biochemical fractionations separating plasma membrane, cytoplasm and endomembrane compartments 23 demonstrated the presence of FAK in EEA1, Rab21 and  $\beta$ 1-integrin-positive endosomal fractions (Fig. 2b). Interestingly, corresponding to the presence of active integrin receptors in endosomes, the integrin activator and focal adhesion component talin, but not paxillin and only very low levels of vinculin, was also detected in endosomes suggesting the recruitment of a specific subset of integrin adhesome proteins to endosomes.

### **Endocytosis contributes to integrin signalling**

Next, we set out to investigate whether the endosome-associated active integrin and FAK are crucial components of integrin-ECM-induced signalling. Serum-starved cells were maintained in suspension for 1 hour (to inactivate RTKs and adhesion-induced pathways) and subsequently plated on integrin ligands. Under these conditions, ECM engagement induced time-dependent activation of the canonical downstream integrin signalling mediators including FAK, ERK1/2 and Akt without significant adhesion-dependent activation of any of the 48 different RTKs tested (Supplementary Fig. 2a, b), suggesting that the observed signals were a consequence of integrin-mediated adhesion and not due to growth factor receptor stimulation. Dynasore-mediated inhibition of dynamin 24, an important mediator of integrin receptor endocytosis 16, abrogated integrin and transferrin receptor internalisation (Supplementary Fig. 3a-c) and significantly attenuated the activation of FAK and ERK1/2 in carcinoma cells and in normal fibroblasts spreading on collagen or fibronectin (Fig. 3a-d and Supplementary Fig. 4a-d) suggesting that endocytosis was key for

adhesion-induced signalling. These results were recapitulated with another dynamin inhibitor Dyngo4 25 and a dynamin dominant-negative construct (Dynamin-2<sup>K44A</sup>-GFP; 26) (Supplementary Fig. 4e, f). Interestingly, not all integrin-mediated pathways, such as Src activation, were consistently inhibited upon defective dynamin function (Fig. 3a-d; Supplementary Fig. 4a-d). This may be attributed to increased integrin plasma-membrane signalling supported by the slightly elevated cell surface  $\beta$ 1-integrin levels in dynamin-inhibited cells (Supplementary Fig. 4g). In line with these data, dynamin inhibition triggered a reduction in the in situ Proximity Ligation Assay (PLA) signal between integrin and pFAK specifically in endosomes and promoted a converse increase in the plasma membrane-localised integrin-pFAK PLA signal (Fig. 3e). In addition, reduced endosomal pFAK and pAkt (another marker of downstream integrin signalling) levels, following dynasore treatment, were confirmed by subcellular fractionation (Supplementary Fig. 4h).

### Integrin endosomal signalling is Rab21 dependent

As dynamin inhibition blocks several cellular endocytic routes we next used siRNA-mediated silencing of Rab21, which interacts directly with the integrin  $\alpha$ -subunit cytoplasmic tail (residues K1160/R1161), as a more direct mechanism to target integrin endocytosis and traffic 9, 27. RNAi-mediated silencing of Rab21 27 significantly reduced FAK phosphorylation (Fig. 3f) upon matrix engagement corresponding with decreased integrin endocytosis observed in Rab21-depleted cells 9. Furthermore, adhesion-induced signalling (pFAK levels) was significantly impaired in cells expressing an endocytosis-defective collagen-binding integrin ( $\alpha$ 2-subunit KR1160/61AA mutation as compared to wild-type  $\alpha$ 2-integrin receptor expressing cells adhering to collagen 28 (Fig. 3g). Taken together, these data demonstrate that impaired integrin endocytosis attenuates adhesion-induced FAK activation.

### FAK is recruited to and activated on purified endosomes

The requirement for endocytosis for enhanced integrin signalling could be linked to sustained signalling of plasma membrane initiated signalling on the endosomes or the ability of integrins to trigger signalling from endomembranes. To study this further we isolated endosomes from FAK<sup>+/+</sup> and FAK<sup>-/-</sup> MEFs.  $\beta$ 1-integrin localised to endosomal and plasma membrane fractions in both cell types indicating that integrin endosomal localisation is not FAK dependent (Fig. 4a). As we found that endosomes contain a subset of integrin signalling components (Fig. 2b) we next addressed the possibility that these components could assemble directly on the endosome. We incubated isolated integrin-containing endosomes, from FAK<sup>-/-</sup> cells, with purified recombinant FAK protein. Strikingly, soluble FAK was specifically recruited to the endosomes, independently of its phosphorylation status (Fig. 4b). Integrins contribute to this recruitment since silencing of  $\beta$ 1-integrins reduced the amount of recruited active FAK (Fig. 4c and Supplementary Fig. 4i). Finally, the non-phosphorylated recombinant FAK became phosphorylated on Y397 on the isolated endosomes *in vitro* (Fig. 4d), suggesting the possibility that internalised integrins could assemble endosomal signalling complexes distinct from the plasma-membrane localised adhesions. This notion was further supported by the observation that exogenous focal adhesion targeting domain of FAK alone (FAK FAT) was unable to localize to the endosomal fraction whereas the endogenous FAK and the FERM-domain of FAK (FAK

FERM) localized to the endosomal fraction (Fig. 4e). Taken together, these data suggest a role for endocytosis in enhancing and possibly triggering distinct integrin downstream signalling events, including FAK activation.

Integrin endocytosis is intimately coupled to the cellular cytoskeleton and cell spreading. In line with this, we observed slightly reduced cell spreading in dynasore-treated cells after 45 min of adhesion to collagen (Supplementary Fig. 5a, b). To exclude the possibility that attenuated adhesion-signalling, upon inhibition of integrin endocytosis, was secondary to alterations in adhesion area, we induced integrin-ECM ligation in suspension using small collagen-coated beads. Dynasore treatment significantly inhibited FAK activation upon cell binding to collagen beads (Supplementary Fig. 5c), indicative of a cell spreading independent regulatory role for endocytosis in ECM-induced integrin signalling. In addition, we found that cell adhesion to round micropatterns with restricted dimensions that constrain cell spreading, supported FAK activation in an endocytosis dependent manner (Fig. 4f).

### Integrin and FAK-proximal proteins on endosomes

To gain further insight into the integrin and FAK signalling networks on the endomembranes we carried out mass spectrometric (MS) analyses of the cytoplasmic, plasma membrane and endosomal fractions of fibroblasts (Fig 5a-d and Supplementary Table 1). Importantly, integrin ligands fibronectin and collagen as well as many established endomembrane proteins, in addition to classic endosome markers, EHD1, Rab14 and rabaptin-5, were detected in the endosomal fraction (Fig. 5b and Supplementary Table 1). Interestingly, 69 proteins identified in the endosomal fraction are components of the literature-curated map of adhesion complexes 29 (Supplementary Table 1) and many more endosome fraction proteins were identified as adhesion components in several published MS datasets (Supplementary Table 1 and materials and methods for details). To highlight putative regulators of FAK or  $\beta$ 1-integrin on endosomes, proteins identified in the endosomal fraction were mapped onto a human protein-protein interaction network and sub-networks containing FAK (Fig. 5c) and  $\beta$ 1-integrin (Fig. 5d) binders were created.

The proteins in both networks have very interesting activities that are likely to contribute to integrin signalling and maintenance of receptor activity. These included actin-binding proteins, scaffolding proteins, integrin activity regulators (e.g. talin), phosphatases known to contribute to signalling and several guanine nucleotide exchange factors (GEFs) implicated in the regulation of small GTPases Rac and Rho. Interestingly, Src and paxillin, both important components of FAK signalling in focal adhesions, were not abundant in the endomembrane fraction (compared to the plasma membrane or cytosolic fractions; Fig. 5b). These data suggest that integrin signalling on endosomes may involve unique features not present in integrin signalling in focal adhesions.

### Integrin endosomal signalling is EEA1-dependent

We next investigated whether increased integrin traffic could augment signalling. Transient overexpression of Rab5-CA and Rab21, previously reported to increase integrin endocytosis in multiple cell types<sup>9, 28, 30</sup>, significantly promoted adhesion-dependent FAK activation (Supplementary Fig. 6a, b). Active  $\beta$ 1-integrin and pFAK are present on endosomes positive

for endogenous EEA1, a key Rab5 effector 31, 32, associated with both Rab5- and Rab21-positive endosomes 4 (Fig. 1c, Supplementary Fig. 1e) and EEA1 and pFAK localize to GFP-EEA1 positive endosomes in fibroblasts adhering to fibronectin (Supplementary Fig. 6c). Although multiple endosomal signalling pathways are EEA1 dependent, a second class of Rab5-positive, EEA1-negative early endosomes containing one or both of the closely related APPL1 and APPL2 adaptors have also been implicated in signalling 33–35. Silencing of EEA1 with a single siRNA oligonucleotide (Fig. 6a) or an independent siRNA smart pool (Supplementary Fig. 6d) significantly reduced adhesion-induced FAK activation (Fig. 6a) without influencing integrin endocytosis (Fig. 6b). In contrast, silencing of APPL1 had no effect on integrin signalling or endocytosis in response to adhesion (Fig. 6b-c). The recruitment of EEA1 to endosomes requires the generation of phosphatidylinositol 3-phosphate (PI(3)P) and inhibition of phosphoinositide-3-phosphate kinase (PI3K) has been shown to decrease the number of EEA1-containing endosomes while increasing the size of APPL1-positive vesicles 36. Accordingly, treatment of cells with a PI3K inhibitor triggered a reduction in the number of EEA1-positive endosomes without reducing total EEA1 levels and inhibited adhesion-induced FAK activation similarly to dynasore treatment (Fig. 6d-e). Taken together, our results reveal an important role for EEA1 but not APPL1 in integrin endosomal signalling.

### Integrin endosomal signalling inhibits anoikis

A central function for integrin-induced signalling is adhesion-dependent cell survival. Upon detachment, normal cells undergo a specialised form of programmed cell death called anoikis, and canonical integrin-mediated activation of FAK on the plasma membrane has been considered critical for anoikis suppression 12. Upon detachment, serum-starved fibroblasts exhibited relatively fast anoikis and inhibition of integrin endocytosis with dynasore or Dyngo4a significantly increased the fraction of apoptotic cells 5 hours post detachment but had no effect on cell survival in adherent cells (Fig. 7a and Supplementary Fig. 7a). Importantly, dynasore treatment reduced pFAK and induced anoikis sensitivity in FAK<sup>+/+</sup> MEFs in suspension to levels seen in FAK<sup>-/-</sup> MEFs under the same experimental condition; however dynamin inhibition did not further increase apoptosis in FAK<sup>-/-</sup> MEFs (Fig. 7b), indicative of a link between FAK activation and sensitivity to dynasore-induced anoikis. Finally, since EEA1-endosomes (but not APPL-endosomes) and Rab21 mediated endocytosis were identified as critical contributors to integrin endosomal FAK signalling (Fig. 3h, 2f), we tested the effect of EEA1, APPL-1 and Rab21 silencing on anoikis sensitivity. RNAi transfections increased the proportion of apoptotic cells to some extent in all siRNA transfected adherent cells (Fig. 4d, e). However, upon cell detachment EEA1- and Rab21-silenced cells showed significantly higher anoikis sensitivity and reduced pFAK levels (Fig. 7c-d, 6a, 3f), whereas APPL1 silencing did not significantly increase anoikis (Supplementary Fig. 7b). Next we tested whether impairment of integrin signalling from endosomes negatively affects the ability of anoikis-resistant cells to grow in an anchorage-independent manner, which is a critical hallmark of cancer. We found that anchorage-independent growth of tumorigenic MDA-MB-231 cells was sensitive to FAK and dynamin inhibition (Supplementary Fig. 8a), suggesting the suitability of these cells for investigation of the functional contribution of endosomal FAK signalling. *In vitro*, silencing of EEA1 and even more significantly silencing of Rab21 reduced the proportion of live cells in suspension

cultures (Fig. 7e). Since anchorage-independent growth has been linked to metastasis 37 we investigated the ability of MDA-MB-231 cells to survive in vasculature and metastasise to lungs. When control and Rab21 siRNA or control and EEA1 transfected cells were co-injected into the same recipient animals, the number of extravasated Rab21-silenced cells in the lung tissue was significantly lower after 48 hours (Fig. 7f-g and Supplementary Fig. 8b). Thus, impaired integrin endosomal signalling sensitises cancer cells to detachment-induced cell death and impairs their metastatic potential *in vivo*.

## Discussion

Our study provides evidence, using multiple complementary approaches, for a non-canonical  $\beta$ 1-integrin signalling that is distinct from the signalling role of integrins in adhesion sites at the plasma membrane (Fig. 8). Our data indicate that active integrins bound to their ligands co-localize with active FAK in endosomes away from the plasma membrane. Integrin-positive endosomes contain talin which may function to maintain the integrin active. In addition, several other signalling and scaffolding proteins are detected in the isolated endosomal fraction and their functional contribution to integrin endosomal signalling will be interesting to investigate in detail in the future. We find that integrin-containing endosomes harbour the capacity to recruit and activate soluble FAK suggesting that a subset of integrin-associated proteins, present in cell-ECM adhesions, may form the core integrin signalling platform in endosomes. It is also possible that active phosphorylated FAK is co-endocytosed with integrin receptors from the plasma membrane and that additional pFAK recruitment to the endosome acts to reinforce signalling downstream of integrin-ECM engagement. Differentiating between these two distinct mechanisms, co-endocytosis or reassembly of integrin-signalling complexes at the endosome, will be crucial for our understanding of integrin endosomal signalling and will require further comprehensive investigation. Nevertheless, integrin signalling from EEA1 endosomes, revealed in this study, functions to accentuate adhesion-induced signalling and facilitates extended survival in anoikis-sensitive cells. Interestingly, the targeting of FAK to endosomes seems to be distinct from its focal adhesion recruitment 38. The focal adhesion targeting sequence (FAT) in FAK is sufficient alone to localize to focal adhesions in cells, however, we find that localization to the endosomes is mediated by the FAK-FERM domain and not the FAT-domain. Furthermore, Src which is a critical enhancer of FAK activity and its down-stream signalling in focal adhesions 39 is only very weakly detectable in the integrin-containing endosomal fractions. Thus, targeting and activation of FAK on endosomes may be mechanistically distinct to from its regulation in focal adhesions.

We show here that endosome-localised active integrin and FAK signalling contribute to cancer-related processes such as anchorage independent growth and metastasis. In the future, unravelling mechanisms involved in the endosomal activation of FAK in non-adherent cells may uncover possible therapeutic targets in anoikis-resistant transformed cells.

## Methods

### Cells

The following cell lines were used in this study: MDA-MB-231 (human breast adenocarcinoma) maintained in DMEM containing 1% MEM nonessential amino acids, 1% L-glutamine and 10% foetal bovine serum (FBS); NCI-H460 (human non-small cell lung carcinoma) in RPMI-1640 (R5886 Sigma) containing 10% FBS, 1% L-glutamine, 1% sodium pyruvate, 1% HEPES (1M) and 1% glucose (45%) and; TIFFs (human telomerase-immortalized foreskin fibroblasts, a gift from Jim Norman) maintained in DMEM containing 1% L-glutamine, 2% HEPES (1M) and 20% FBS; CHO (Chinese hamster ovary cells) in Alpha-MEM (M4526, Sigma) containing 1% L-glutamine and 5% FBS; GD25- $\beta$ 1A (mouse fibroblasts, described in 40) cultured in DMEM containing 1% L-glutamine, 10% FBS and 10  $\mu$ g/ml puromycin and FAK<sup>-/-</sup> and FAK<sup>+/+</sup> MEFs (mouse embryonic fibroblasts provided by D. Schlaepfer UCSF, described in 41) cultured in DMEM containing 10% FBS, 100 U/ml penicillin, 100  $\mu$ g/ml streptomycin, 1% MEM nonessential amino acids, 1% sodium pyruvate and 1% L-glutamine. DMEM was from Sigma (D5796). Unless otherwise indicated, the cell lines were obtained from American Type Culture Collection (ATCC). The cell lines used in this study are not found in the ICLAC database for cross-contaminated or otherwise misidentified cell lines, and were not authenticated. All cells were serum starved for 24 h before all experiments unless otherwise indicated. All cells were routinely tested for mycoplasma contamination. All experiments were repeated at least three times unless otherwise indicated.

### Antibodies & reagents

A detailed list of used primary antibodies is provided in Supplementary Table 3. Phalloidin-Atto 647N (65906-10NMOL) was purchased from Fluka; AlexaFluor-conjugated secondary antibodies (488, 555, 647 conjugated anti-mouse, rabbit and rat antibodies) were purchased from Life Technologies; Mega-520 (rabbit) and Atto-647 (mouse) secondary antibodies for STED were from Sigma; secondary antibodies for detecting immunoblots with Odyssey (DyLight 680 and 800 conjugated anti-mouse, rabbit and rat antibodies) were from Thermo Scientific. Live-cell dyes, Far red DDAO-SE and green CMFDA were obtained from Molecular Probes. Dynasore monohydrate (D7693), DMSO (D2650) and collagen type I solution (C8919) were obtained from Sigma. Dyngo4a was from Abcam (ab120689) and FAK-inhibitors PF-562271 (S2890) and PF-573228 (S2013) were obtained from Selleckchem. CellPlayer 96-Well Kinetic Caspase-3/7 Apoptosis Assay Kit (Nucview, 4440) was purchased from Essen Bioscience, LY294002 (PHZ1144) and AlexaFluor568 conjugated transferrin (T-23365) from Life Technologies, fibronectin bovine plasma (341631) from Merck and Polybead® Microspheres 6.00  $\mu$ m (07312-5) from Polysciences. FAK inhibitor 14 (3414) and Human Phospho-RTK Array (ARY001) were from R&D Systems. Active (0165-0000-3) and non-activated (0165-0000-1) recombinant FAK were purchased from ProQinase. pET15b-FNIII (7-10) was a gift from Reinhard Fässler. HyQTase (SV30030.01) from HyClone was used to detach cells for re-plating before start of experiment.



## siRNAs and plasmids

The following siRNAs and their target sequences were used (all from Qiagen): Allstars negative control siRNA (1027281); siEEA1, ATGGATAACATGACCTTGGA; EEA1 smart pool (three siRNAs), AGCCGCTATATTAGACTTGA, AAGCTAAGTTGCATTCCGAAA, CCCGGCACAGAATGTGAGTTA; si $\beta$ 1-integrin, CCCGACATCATCCCAATTGTA, and CTGGTCCATGTCTAGCGTCAA; siRab21, AAGGCATCATTCTTAACAAAG (3'-Alexa Fluor 555) and siAPPL1, CAGGACAATCTCGGCCACCGA. The following plasmids were used: pEGFP-C1 (Clontech), GFP-Rab5-Q79L and GFP-Rab21 9, pIRES-GFP- $\alpha$ 2 WT/- $\alpha$ 2-AA 28, GFP-Dyn2K44A 42, GFP-EEA1 (Addgene plasmid 42307 43), GFP-FAK wt, GFP-FAK FERM (1-402) and GFP-FAK FAT from David Schlaepfer. Lipofectamine 2000 (11668-019, Life Technologies) and HiPerfect (301705, Qiagen) were used for transient transfections and siRNA silencing according to manufacturer's protocol.

## Subcellular fractionation

The protocol was modified from 23. Briefly, adherent cells were scraped on ice into hypotonic lysis buffer (10 mM HEPES-KOH pH 7.2, 0.25 M sucrose, 1 mM EDTA, 1 mM MgOAc and protease & phosphatase inhibitors (PhosSTOP and Complete mini tablets from Roche). Cell membranes were fragmented with French Press and nuclei removed with 10 min 1000 x g centrifugation. Plasma membrane fraction was collected with 10 min 10,000 x g centrifugation and endosomal/cytoplasmic fractions with 1 h 100,000 x g centrifugation. Membrane fractions were washed at least once with lysis buffer and cytoplasmic fractions were centrifuged twice. All fractionation steps were performed at +4°C or on ice. All fractions were dissolved in sample buffer for immunoblotting. Direct protein binding to isolated endosomes was assessed with recombinant proteins. Therefore, the endosomal fraction derived from FAK<sup>-/-</sup> MEFs was resuspended in buffer containing 20 mM Tris-HCl pH 7.4, 150 mM NaCl, 1 mM MgCl<sub>2</sub>, 1 mM DTT and protease & phosphatase inhibitors and subsequently incubated with 0.5  $\mu$ g of either phosphorylated or non-phosphorylated FAK (ProKinase) or GST for 2 h at room temperature. In order to assess whether FAK can be activated on endosomes in vitro, GST or non-phosphorylated FAK were incubated for 1.5 h with the purified endosomes and then 10  $\mu$ M ATP was added or not for another 30 min. Following 100,000 x g centrifugation for 1 h, the total soluble (supernatant) and non-soluble endosomal (pellet) fractions were analysed by SDS-PAGE followed by western blotting with the indicated antibodies.

## In-situ Proximity ligation assay (PLA)

PLA was done according to manufacturer's protocol (Duolink, Olink BioScience) in serum starved TIFFs plated on collagen for 45 min +/- dynasore followed by 4% PFA + 1 mM MgCl<sub>2</sub> fixing.

## Replating assay: integrin activation by ligand engagement

The same protocol was used in all experiments where integrin signalling was activated by integrin ligand engagement at different time points. Cells were serum starved for 24h, detached with HyQTase, washed and kept in suspension in serum-free medium for 1 h to

stop adhesion signalling. Dynasore (80  $\mu\text{M}$  44, 45), LY294002 (40  $\mu\text{M}$ ), Dyngo4a (10  $\mu\text{M}$ ) or equal volumes of DMSO were added to cells 15 min before replating on collagen type I or fibronectin-coated (5  $\mu\text{g}/\text{ml}$ ) dishes or coverslips for different time points at +37°C. Cells were washed with cold PBS and collected on ice for immunoblotting.

### **Inhibitor assay**

Adherent unstarved cells were treated with FAK inhibitors (10  $\mu\text{M}$  of FAK-14, 1  $\mu\text{M}$  of PF271 or 1  $\mu\text{M}$  of PF228) for 3h at +37°C after which the cells were either fixed and stained for immunofluorescence or collected in sample buffer for immunoblotting.

### **Immunoblotting**

Immunoblotting was performed by using standard western blotting techniques and either ECL detection or Odyssey LICOR imaging system. The level of phosphorylated proteins was quantified by measuring the integrated band intensities with NIH ImageJ (1.45s) and unless otherwise indicated, band intensities of phospho-proteins were normalised to the corresponding tubulin band and to the sum of all time points inside an experiment.

### **Flow cytometric assay**

Cells were treated as described in replating assay with the exception that in the end cells were detached with HyQTase, washed and fixed. Fixing and staining of the cells was performed as described in 46.

### **Bead assay**

Beads (6  $\mu\text{m}$ , Polybead® Microspheres,) were coated with 10  $\mu\text{g}/\text{ml}$  collagen in 2% BSA for 2 h at +37°C and blocked with 2% BSA/PBS for 1h at RT. Serum-starved cells were treated with DMSO or dynasore as described in the replating assays, mixed with coated beads in low-attachment 6-well cell culture dishes (Corning Costar Ultra-Low attachment 6 well plate, CLS3471, Corning) and incubated at +37°C for 45 min. Cold PBS was added to the wells, cells with beads were collected on ice, centrifuged at 210 x g for 3 min at +4°C and resuspended in sample buffer for immunoblotting.

### **Anoikis assay**

Adherent, serum-starved cells were treated with 80  $\mu\text{M}$  dynasore, 3 or 10  $\mu\text{M}$  dyngo4a or equivalent amounts of DMSO for 1 h at +37°C. Cells were maintained at +37°C for 5 h or detached with HyQTase, washed and suspended in 5 ml of serum-free medium containing the same concentrations of dynasore or Dyngo4a and kept in suspension for 5h at +37°C. Adherent cells were collected with HyQTase and all cells were then analysed for the Caspase-3/7 positivity using Nucview Apoptosis Assay according to manufacturer's protocol (Essen Bioscience).

### **Immunofluorescence, microscopy, image and co-distribution analysis**

Cells plated on Ibidi dishes (Integrated Biodiagnostics) or on acid washed coverslips were fixed with 4% paraformaldehyde (PFA) containing 1mm  $\text{MgCl}_2$  for 15 min at RT and permeabilised with 0.2% Triton-X-100 in 30% horse serum/TBS for 15 min at RT. Samples

were blocked and antibodies were diluted in 30% horse serum/TBS. Primary antibodies were used at predetermined concentrations (5-10 µg/ml) and AlexaFluor secondary antibodies as 5 µg/ml. Unless otherwise stated, all images were acquired using the spinning disc confocal microscope as described 7 with the exception of 100×/1.3 Oil (Pha3, EC Plan Neofluar) objective being used. The microscope, image acquisition and related data analysis for the crossbow-shaped micropatterns is described 18. Quantitative analysis for all other images was performed using NIH ImageJ (1.45s). Following background subtraction,  $\beta$ 1 integrin and 555-Trf endocytosis was calculated from mid-slices by measuring the integrated density within the cell as a percentage of the total integrated density (integrin endocytosis) or by measuring the mean intensity of the cell (Trf endocytosis). Leica TCS SP5 Stimulated Emission Depletion (STED) laser scanning microscope was used to acquire images in super-resolution level (Leica Microsystems GmbH, Mannheim, Germany), where approximately 65 nm resolution in x,y -axis was achieved. Leica STED IR corrected objective 100×/1.4 was used. Mega-520 fluorophore was excited at 532 nm wavelength (PicoQuant, Berlin, Germany) and Star-635 at 635 nm wavelength (PicoQuant, Berlin, Germany). The channels were scanned sequentially and emission was detected by avalanche photodiode detectors at the emission range of 685/40 (Leica Microsystems GmbH, Mannheim, Germany). Leica LAS software (Leica Microsystems GmbH, Mannheim, Germany) was used to perform background subtraction and deconvolution in all images. In the deconvolution process a Lorentzian PSF was generated by using the measured PSF value of 62 nm, which was exploited to signal energy based deconvolution algorithm. GFP-Rab5-CA was imaged with confocal resolution, by using 488 nm laser line for excitation, and emission was detected at 500-530 nm. In the deconvolution process a Gaussian PSF was generated for the confocal channel by using the measured PSF value of 230 nm, which was exploited to signal energy based deconvolution algorithm. STED imaging was performed at the Laboratory of Biophysics, University of Turku. Image colocalisation analysis was done by using the Intensity Correlation Analysis plugin for ImageJ to create PDM (product of the differences from the mean) images, where  $PDM = (\text{red intensity} - \text{mean red intensity}) \times (\text{green intensity} - \text{mean green intensity})$ . Analysis of co-distribution between active  $\beta$ 1-integrin and pFAK puncta on microdomains of either Rab5-, Rab21- or EEA1-positive endosomes, was performed as described in 15. The distance between pFAK and FAK was measured by selecting a random non-endosomal pFAK puncta and measuring the distance to closest neighbour pFAK puncta.

### **Micropatterns and probabilistic density maps**

Micropatterns were produced on glass coverslips as described in 47. Cells were seeded on micropatterns in serum-free medium for either 3h or 45 min (cells on spots) before fixing. Samples were stained as described above. The microscope, image acquisition and creation of the probabilistic density maps are described in 18.

### **Mice**

Eight weeks old female Hsd:Athymic Nude - Foxn1nu mice were used for animal experiments. Studies were performed under a valid animal license (license number 4199/04.10.07/2014) and conducted according to the Finnish act on animal experimentation-guidelines.

## Lung extravasation

Control and Rab21 or EEA1 siRNA transfected MDA-MB-231 cells were labelled with live cell dyes (siCtrl: Far red DDAO-SE; siRab21/EEA1: green CMFDA) according to the manufacturer's instructions. siControl- and siRab21/siEEA1-treated cells ( $0.75 \times 10^6$  cells each) were injected in a 1:1 ratio in the tail vein of 15 mice and lungs were collected 48 h after injection. This animal number has previously been sufficient for statistical significance in a similar experimental set-up 48,49. The left lung of each mouse was formalin fixed and processed for frozen sections to be analysed by fluorescence microscopy and right lungs were processed into a cell suspension by Collagenase I treatment as described in 48, 49 and the number of fluorescently labelled cells was analyzed by flow cytometry using LSRFortessa™ from BD Biosciences. The analyses were blinded such that the investigator analyzing the data was unaware of the identity of the labelled cell populations. The quantitation shows the ratio of siCtrl- and siRab21- or EEA1-treated cells in each lung. No blinding or randomization was performed as both cell types are co-injected in the same recipient animals simultaneously and analysed from the same samples using flow cytometry.

## Mass spectrometry

Protein samples obtained from subcellular fractionation of WT MEFs were separated by SDS-PAGE and allowed to migrate 20 mm into a 4–12% polyacrylamide gel. Following staining with InstantBlue (Expedeon), gel lanes were sliced into ten 2-mm bands and subjected to in-gel digestion with trypsin as described previously 50 with modifications. Tryptic peptides were evaporated to dryness, dissolved in 1% HCOOH and 5  $\mu$ l was submitted to LC-MS/MS analysis. The LC-MS/MS analysis was performed on a nanoflow HPLC system (EasyNano, Thermo Fisher Scientific) coupled to the LTQ Orbitrap Velos Pro mass spectrometer (Thermo Fisher Scientific, Bremen, Germany) equipped with a nano-electrospray ionization source. Peptides were first loaded on a trapping column and subsequently separated inline on a 15 cm C<sub>18</sub> column (75  $\mu$ m x 15 cm, Magic 5  $\mu$ m 200 Å C<sub>18</sub>, Michrom BioResources Inc., Sacramento, CA, USA). The mobile phase consisted of water/acetonitrile (98:2 (v/v)) with 0.2% formic acid (solvent A) or acetonitrile/water (95:5 (v/v)) with 0.2% formic acid (solvent B). A linear 50 min gradient from 5% to 35% B was used to elute peptides.

MS data was acquired automatically using Thermo Xcalibur software (Thermo Fisher Scientific). An information dependent acquisition method consisted of a TOF MS survey scan of mass range 300-2000 m/z. The data files were searched for protein identification using Proteome Discoverer (1.4) connected to in-house Mascot (v. 2.4) software. Data was searched against the SwissProt database (release 2014\_08). Carbamidomethylation of cysteine was set as a fixed modification and oxidation of methionine was allowed as a variable modification. Only tryptic peptides were considered, with up to one missed cleavage permitted. Monoisotopic precursor mass values were used, and only doubly and triply charged precursor ions were considered. Data were validated in Scaffold (version 3.6) using a threshold of identification of at least 50% probability at the peptide level, at least 99% probability at the protein level and assignment of at least two unique, validated peptides. These acceptance criteria resulted in an estimated protein false discovery rate of 0.1% for all datasets.

Data were converted using PRIDE Converter 2 51, validated using PRIDE Inspector (version 2.5) 52. Details of all identified proteins are provided in supplementary material Tables S1.

Proteins identified in the various cellular fractions and described to be components of the Geiger Adhesome 29 were hierarchically clustered on the basis of uncentred Pearson correlation using Cluster 3.0 (C Clustering Library, version 1.50) 53 and visualised using Java TreeView (version 1.1.6r2) 54. Protein-protein interaction (PPIs) network analysis was performed using Cytoscape (version 3.2) 55. Proteins were mapped onto a merged human interactome consisting of PPIs reported in the Protein Interaction Network Analysis platform Homo sapiens network (May 2014) 56. Identified proteins were also compared to the proteins identified in various published dataset of isolated adhesion complexes 57–61.

### Accession numbers

The proteomic data are deposited in the PRIDE database (<http://www.ebi.ac.uk/pride>) 62 under project accession no. PXD001870 and project DOI: [10.6019/PXD001870](https://doi.org/10.6019/PXD001870).

### Statistics

The data sets with sufficient n numbers to run the D'Agostino & Pearson Omnibus were all found to be normally distributed, therefore these data were analysed using unpaired Student's t-test. For data sets that the n numbers were too small for D'Agostino & Pearson Omnibus normality test, we assumed normal distribution based on the appearance of the data. Statistical significance was analysed using Student's t-test with normal distribution and equal variance.  $P < 0.05 = *$ ,  $p < 0.01 = **$ ,  $p < 0.005 = ***$ . No statistical method was used to predetermine sample size.

### Supplementary Material

Refer to Web version on PubMed Central for supplementary material.

### Acknowledgements

We thank J. Siivonen and P. Laasola for excellent technical assistance, M. Georgiadou, D. Schlaepfer and J. Heino for insightful comments on the manuscript and H. Hamidi for scientific writing and editing of the manuscript. S. Corvera is acknowledged for GFP-EEA1 plasmid (Addgene), Prof. David Schlaepfer for the FAK wt and -/- MEFs and the GFP-FAK plasmids, T. Närejoja and S. Koho for assistance with the STED instrument, Cell Imaging Core facility, University of Turku Centre for Biotechnology, and the Nikon Imaging Centre at Institut Curie-CNRS for help with the imaging. Turku Centre for Disease Modelling is acknowledged for help with the metastasis assays. This study has been supported by the Academy of Finland, ERC Starting Grant, ERC Consolidator Grant, the Sigrid Juselius Foundation, and the Finnish Cancer Organization. J.A. has been supported by the Turku Doctoral Program of Biomedical Sciences and an EMBO Short-Term Fellowship. G.J is supported by an EMBO Long-Term Fellowship.

### References

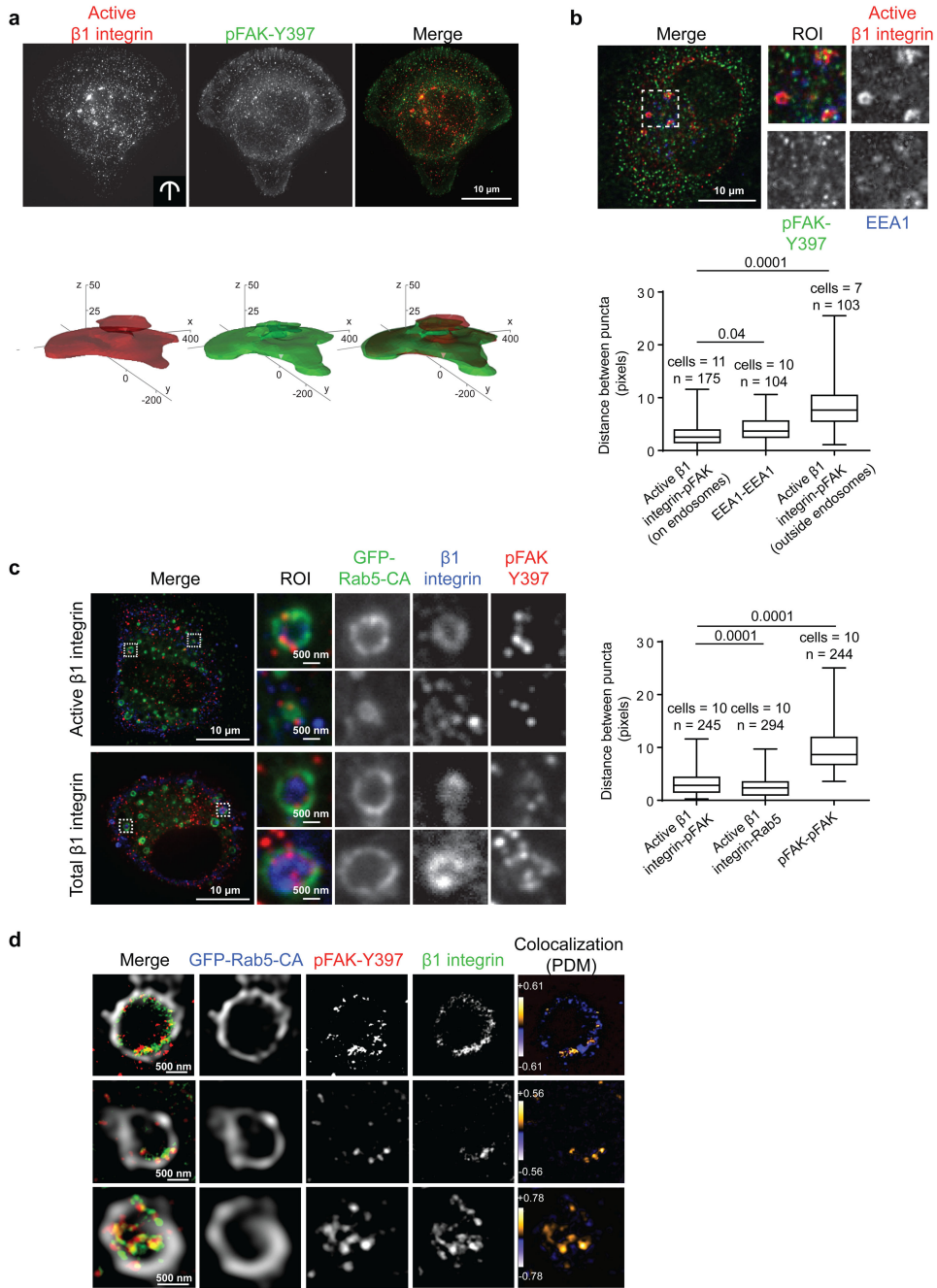
1. Harburger DS, Calderwood DA. Integrin signalling at a glance. *J Cell Sci.* 2009; 122:159–163. [PubMed: 19118207]
2. Winograd-Katz SE, Fassler R, Geiger B, Legate KR. The integrin adhesome: from genes and proteins to human disease. *Nat Rev Mol Cell Biol.* 2014; 15:273–288. [PubMed: 24651544]
3. Zaidel-Bar R, Itzkovitz S, Ma'ayan A, Iyengar R, Geiger B. Functional atlas of the integrin adhesome. *Nat Cell Biol.* 2007; 9:858–867. [PubMed: 17671451]

4. De Franceschi N, Hamidi H, Alanko J, Sahgal P, Ivaska J. Integrin traffic - the update. *J Cell Sci.* 2015; 128:839–852. [PubMed: 25663697]
5. Ceresa BP, Schmid SL. Regulation of signal transduction by endocytosis. *Curr Opin Cell Biol.* 2000; 12:204–210. [PubMed: 10712919]
6. Scita G, Di Fiore PP. The endocytic matrix. *Nature.* 2010; 463:464–473. [PubMed: 20110990]
7. Arjonen A, Alanko J, Veltel S, Ivaska J. Distinct recycling of active and inactive beta1 integrins. *Traffic.* 2012; 13:610–625. [PubMed: 22222055]
8. Dozynkiewicz MA, et al. Rab25 and CLIC3 collaborate to promote integrin recycling from late endosomes/lysosomes and drive cancer progression. *Dev Cell.* 2012; 22:131–145. [PubMed: 22197222]
9. Pellinen T, et al. Small GTPase Rab21 regulates cell adhesion and controls endosomal traffic of beta1-integrins. *J Cell Biol.* 2006; 173:767–780. [PubMed: 16754960]
10. Muller PA, et al. Mutant p53 drives invasion by promoting integrin recycling. *Cell.* 2009; 139:1327–1341. [PubMed: 20064378]
11. Muller PA, et al. Mutant p53 enhances MET trafficking and signalling to drive cell scattering and invasion. *Oncogene.* 2013; 32:1252–1265. [PubMed: 22580601]
12. Frisch SM, Vuori K, Ruoslahti E, Chan-Hui PY. Control of adhesion-dependent cell survival by focal adhesion kinase. *J Cell Biol.* 1996; 134:793–799. [PubMed: 8707856]
13. Geiger B, Bershadsky A, Pankov R, Yamada KM. Transmembrane crosstalk between the extracellular matrix--cytoskeleton crosstalk. *Nat Rev Mol Cell Biol.* 2001; 2:793–805. [PubMed: 11715046]
14. Hynes RO. The extracellular matrix: not just pretty fibrils. *Science.* 2009; 326:1216–1219. [PubMed: 19965464]
15. Bridgewater RE, Norman JC, Caswell PT. Integrin trafficking at a glance. *J Cell Sci.* 2012; 125:3695–3701. [PubMed: 23027580]
16. Caswell PT, Vadrevu S, Norman JC. Integrins: masters and slaves of endocytic transport. *Nat Rev Mol Cell Biol.* 2009; 10:843–853. [PubMed: 19904298]
17. Brunton VG, Frame MC. Src and focal adhesion kinase as therapeutic targets in cancer. *Curr Opin Pharmacol.* 2008; 8:427–432. [PubMed: 18625340]
18. Schauer K, et al. Probabilistic density maps to study global endomembrane organization. *Nat Methods.* 2010; 7:560–566. [PubMed: 20512144]
19. Stenmark H, et al. Inhibition of rab5 GTPase activity stimulates membrane fusion in endocytosis. *EMBO J.* 1994; 13:1287–1296. [PubMed: 8137813]
20. Lobert VH, et al. Ubiquitination of alpha 5 beta 1 integrin controls fibroblast migration through lysosomal degradation of fibronectin-integrin complexes. *Dev Cell.* 2010; 19:148–159. [PubMed: 20643357]
21. Monteiro P, et al. Endosomal WASH and exocyst complexes control exocytosis of MT1-MMP at invadopodia. *J Cell Biol.* 2013; 203:1063–1079. [PubMed: 24344185]
22. Christoforides C, Rainero E, Brown KK, Norman JC, Toker A. PKD controls alphavbeta3 integrin recycling and tumor cell invasive migration through its substrate Rabaptin-5. *Dev Cell.* 2012; 23:560–572. [PubMed: 22975325]
23. Bass MD, et al. A syndecan-4 hair trigger initiates wound healing through caveolin- and RhoG-regulated integrin endocytosis. *Dev Cell.* 2011; 21:681–693. [PubMed: 21982645]
24. Kirchhausen T, Macia E, Pelish HE. Use of dynasore, the small molecule inhibitor of dynamin, in the regulation of endocytosis. *Methods Enzymol.* 2008; 438:77–93. [PubMed: 18413242]
25. Hill TA, et al. Inhibition of dynamin mediated endocytosis by the dynoles--synthesis and functional activity of a family of indoles. *J Med Chem.* 2009; 52:3762–3773. [PubMed: 19459681]
26. Damke H, Baba T, Warnock DE, Schmid SL. Induction of mutant dynamin specifically blocks endocytic coated vesicle formation. *J Cell Biol.* 1994; 127:915–934. [PubMed: 7962076]
27. Mai A, et al. Competitive binding of Rab21 and p120RasGAP to integrins regulates receptor traffic and migration. *J Cell Biol.* 2011; 194:291–306. [PubMed: 21768288]
28. Pellinen T, et al. Integrin trafficking regulated by Rab21 is necessary for cytokinesis. *Dev Cell.* 2008; 15:371–385. [PubMed: 18804435]

29. Zaidel-Bar R, Geiger B. The switchable integrin adhesome. *J Cell Sci.* 2010; 123:1385–1388. [PubMed: 20410370]
30. Sandri C, et al. The R-Ras/RIN2/Rab5 complex controls endothelial cell adhesion and morphogenesis via active integrin endocytosis and Rac signaling. *Cell Res.* 2012; 22:1479–1501. [PubMed: 22825554]
31. Mu FT, et al. EEA1, an early endosome-associated protein. EEA1 is a conserved alpha-helical peripheral membrane protein flanked by cysteine “fingers” and contains a calmodulin-binding IQ motif. *J Biol Chem.* 1995; 270:13503–13511. [PubMed: 7768953]
32. Christoforidis S, McBride HM, Burgoyne RD, Zerial M. The Rab5 effector EEA1 is a core component of endosome docking. *Nature.* 1999; 397:621–625. [PubMed: 10050856]
33. Erdmann KS, et al. A role of the Lowe syndrome protein OCRL in early steps of the endocytic pathway. *Dev Cell.* 2007; 13:377–390. [PubMed: 17765681]
34. Miaczynska M, et al. APPL proteins link Rab5 to nuclear signal transduction via an endosomal compartment. *Cell.* 2004; 116:445–456. [PubMed: 15016378]
35. Miaczynska M, Pelkmans L, Zerial M. Not just a sink: endosomes in control of signal transduction. *Curr Opin Cell Biol.* 2004; 16:400–406. [PubMed: 15261672]
36. Zoncu R, et al. A phosphoinositide switch controls the maturation and signaling properties of APPL endosomes. *Cell.* 2009; 136:1110–1121. [PubMed: 19303853]
37. Paoli P, Giannoni E, Chiarugi P. Anoikis molecular pathways and its role in cancer progression. *Biochim Biophys Acta.* 2013; 1833:3481–3498. [PubMed: 23830918]
38. Prutzman KC, et al. The focal adhesion targeting domain of focal adhesion kinase contains a hinge region that modulates tyrosine 926 phosphorylation. *Structure.* 2004; 12:881–891. [PubMed: 15130480]
39. Owen JD, Ruest PJ, Fry DW, Hanks SK. Induced focal adhesion kinase (FAK) expression in FAK-null cells enhances cell spreading and migration requiring both auto- and activation loop phosphorylation sites and inhibits adhesion-dependent tyrosine phosphorylation of Pyk2. *Mol Cell Biol.* 1999; 19:4806–4818. [PubMed: 10373530]
40. Wennerberg K, et al. The cytoplasmic tyrosines of integrin subunit beta1 are involved in focal adhesion kinase activation. *Mol Cell Biol.* 2000; 20:5758–5765. [PubMed: 10891511]
41. Schlaepfer DD, et al. Tumor necrosis factor-alpha stimulates focal adhesion kinase activity required for mitogen-activated kinase-associated interleukin 6 expression. *J Biol Chem.* 2007; 282:17450–17459. [PubMed: 17438336]
42. Altschuler Y, et al. Redundant and distinct functions for dynamin-1 and dynamin-2 isoforms. *J Cell Biol.* 1998; 143:1871–1881. [PubMed: 9864361]
43. Lawe DC, Patki V, Heller-Harrison R, Lambright D, Corvera S. The FYVE domain of early endosome antigen 1 is required for both phosphatidylinositol 3-phosphate and Rab5 binding. Critical role of this dual interaction for endosomal localization. *J Biol Chem.* 2000; 275:3699–3705. [PubMed: 10652369]
44. Miyauchi K, Kim Y, Latinovic O, Morozov V, Melikyan GB. HIV enters cells via endocytosis and dynamin-dependent fusion with endosomes. *Cell.* 2009; 137:433–444. [PubMed: 19410541]
45. Macia E, et al. Dynasore, a cell-permeable inhibitor of dynamin. *Dev Cell.* 2006; 10:839–850. [PubMed: 16740485]
46. Virtakoivu R, Pellinen T, Rantala JK, Perala M, Ivaska J. Distinct roles of AKT isoforms in regulating beta1-integrin activity, migration, and invasion in prostate cancer. *Mol Biol Cell.* 2012; 23:3357–3369. [PubMed: 22809628]
47. Azioune A, Storch M, Bornens M, Thery M, Piel M. Simple and rapid process for single cell micro-patterning. *Lab Chip.* 2009; 9:1640–1642. [PubMed: 19458875]
48. Arjonen A, et al. Mutant p53-associated myosin-X upregulation promotes breast cancer invasion and metastasis. *J Clin Invest.* 2014; 124:1069–1082. [PubMed: 24487586]
49. Vuoriluoto K, et al. Vimentin regulates EMT induction by Slug and oncogenic H-Ras and migration by governing Axl expression in breast cancer. *Oncogene.* 2011; 30:1436–1448. [PubMed: 21057535]
50. Shevchenko A, et al. A strategy for identifying gel-separated proteins in sequence databases by MS alone. *Biochem Soc Trans.* 1996; 24:893–896. [PubMed: 8878870]

51. Cote RG, et al. The PRIDE Converter 2 framework: an improved suite of tools to facilitate data submission to the PRIDE database and the ProteomeXchange consortium. *Mol Cell Proteomics*. 2012
52. Wang R, et al. PRIDE Inspector: a tool to visualize and validate MS proteomics data. *Nat Biotech*. 2012; 30:135–137.
53. Hoon, MJLd; Imoto, S.; Nolan, J.; Miyano, S. Open source clustering software. *Bioinformatics*. 2004; 20:1453–1454. [PubMed: 14871861]
54. Saldanha AJ. Java Treeview—extensible visualization of microarray data. *Bioinformatics*. 2004; 20:3246–3248. [PubMed: 15180930]
55. Saito R, et al. A travel guide to Cytoscape plugins. *Nat Methods*. 2012; 9:1069–1076. [PubMed: 23132118]
56. Cowley MJ, et al. PINA v2.0: mining interactome modules. *Nucl Acids Res*. 2012; 40:D862–D865. [PubMed: 22067443]
57. Schiller HB, Friedel CC, Boulegue C, Fässler R. Quantitative proteomics of the integrin adhesome show a myosin II-dependent recruitment of LIM domain proteins. *EMBO Rep*. 2011; 12:259–266. [PubMed: 21311561]
58. Schiller HB, et al.  $\beta$  1- and  $\alpha$ v-class integrins cooperate to regulate myosin II during rigidity sensing of fibronectin-based microenvironments. *Nat Cell Biol*. 2013; 15:625–636. [PubMed: 23708002]
59. Humphries JD, et al. Proteomic analysis of integrin-associated complexes identifies RCC2 as a dual regulator of Rac1 and Arf6. *Sci Signal*. 2009; 2
60. Ng DHJ, Humphries JD, Byron A, Millon-Frémillon A, Humphries MJ. Microtubule-dependent modulation of adhesion complex composition. *PLoS ONE*. 2014; 9
61. Robertson J, et al. Defining the phospho-adhesome through the phosphoproteomic analysis of integrin signalling. *Nat Commun*. 2015; 6
62. Vizcaino JA, et al. The Proteomics Identifications (PRIDE) database and associated tools: status in 2013. 2013; 41:D1063–D1069.

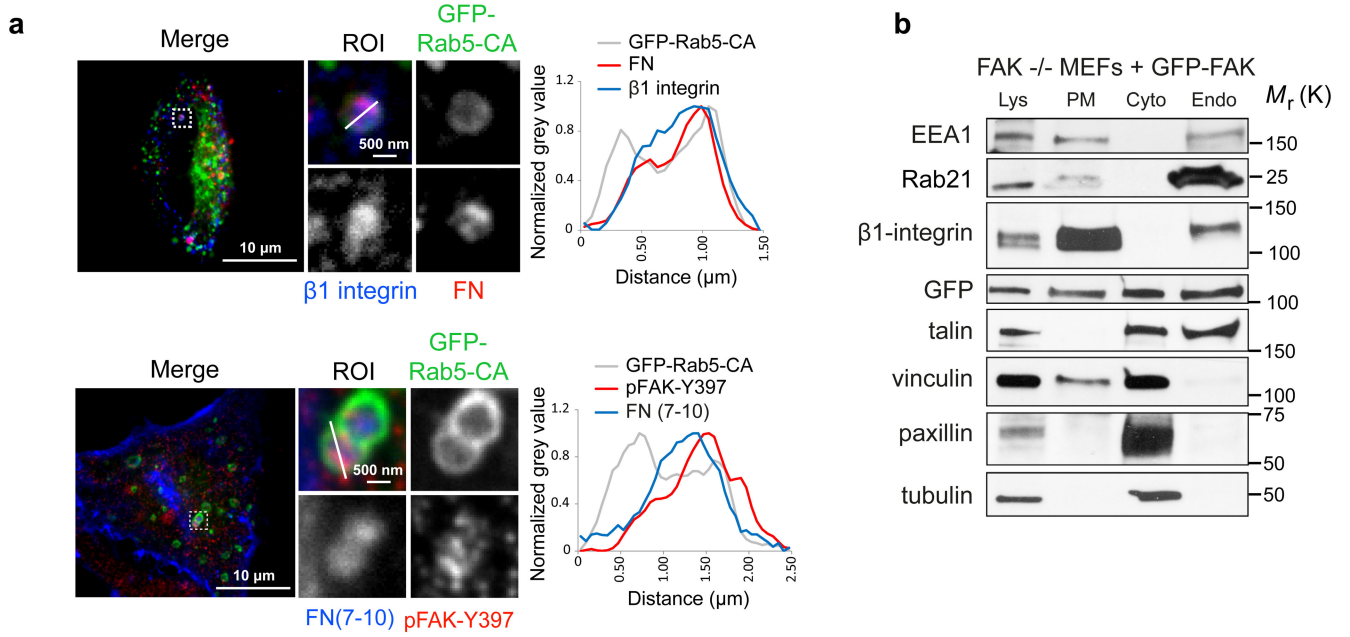




**Figure 1. pFAK-Y397 localizes to endosomes together with  $\beta 1$ -integrin.**

**a**, Representative images and 3D probabilistic density maps of active  $\beta 1$ -integrin and pFAK-Y397 localisation in MDA-MB-231 cells plated on crossbow-shaped fibronectin-coated micropatterns (24 cells assessed in three independent experiments). **b**, Representative confocal images of endogenous active  $\beta 1$ -integrin, pFAK and EEA1 staining in MDA-MB-231 cells and box plot of the distance between adjacent puncta of active  $\beta 1$ -integrin and pFAK in or outside the EEA1-positive endosomes (in pixels) (box plots show the 25th–75th percentiles delineated by the upper and lower limits of the box; the median is shown by the

horizontal line inside the box. Whiskers indicate maxima and minima).  $n$ = the number of active  $\beta$ 1-integrin-pFAK and EEA1-EEA1 doublets (indicated in the figure) analysed from multiple cells (numbers indicated in the figure) from three independent experiments are indicated. **c**, Representative confocal images of pFAK and total or active  $\beta$ 1-integrin staining in GFP-Rab5-CA-expressing TIFFs adhering to fibronectin (45 min). Box plot of the distance between adjacent puncta of active  $\beta$ 1-integrin and pFAK or Rab5 in GFP-Rab5-positive endosomes and between pFAK and pFAK outside the endosomes (in pixels) (box plots show the 25th–75th percentiles delineated by the upper and lower limits of the box; the median is shown by the horizontal line inside the box. Whiskers indicate maxima and minima). Numbers of cells and of active  $\beta$ 1-integrin-pFAK, active  $\beta$ 1-integrin-Rab5 and pFAK-pFAK doublets ( $n$ ) analysed from three independent experiments are indicated. **d**, Super-resolution STED images of active  $\beta$ 1-integrin and pFAK-Y397 on single GFP-Rab5-CA endosomes in TIFFs adhering to fibronectin (45 min). Images displaying PDM (product of the differences from the mean) values were generated to visualize the colocalization between  $\beta$ 1-integrin and pFAK-Y397. ROI: region of interest. Mann-Whitney test  $P$  values are provided.



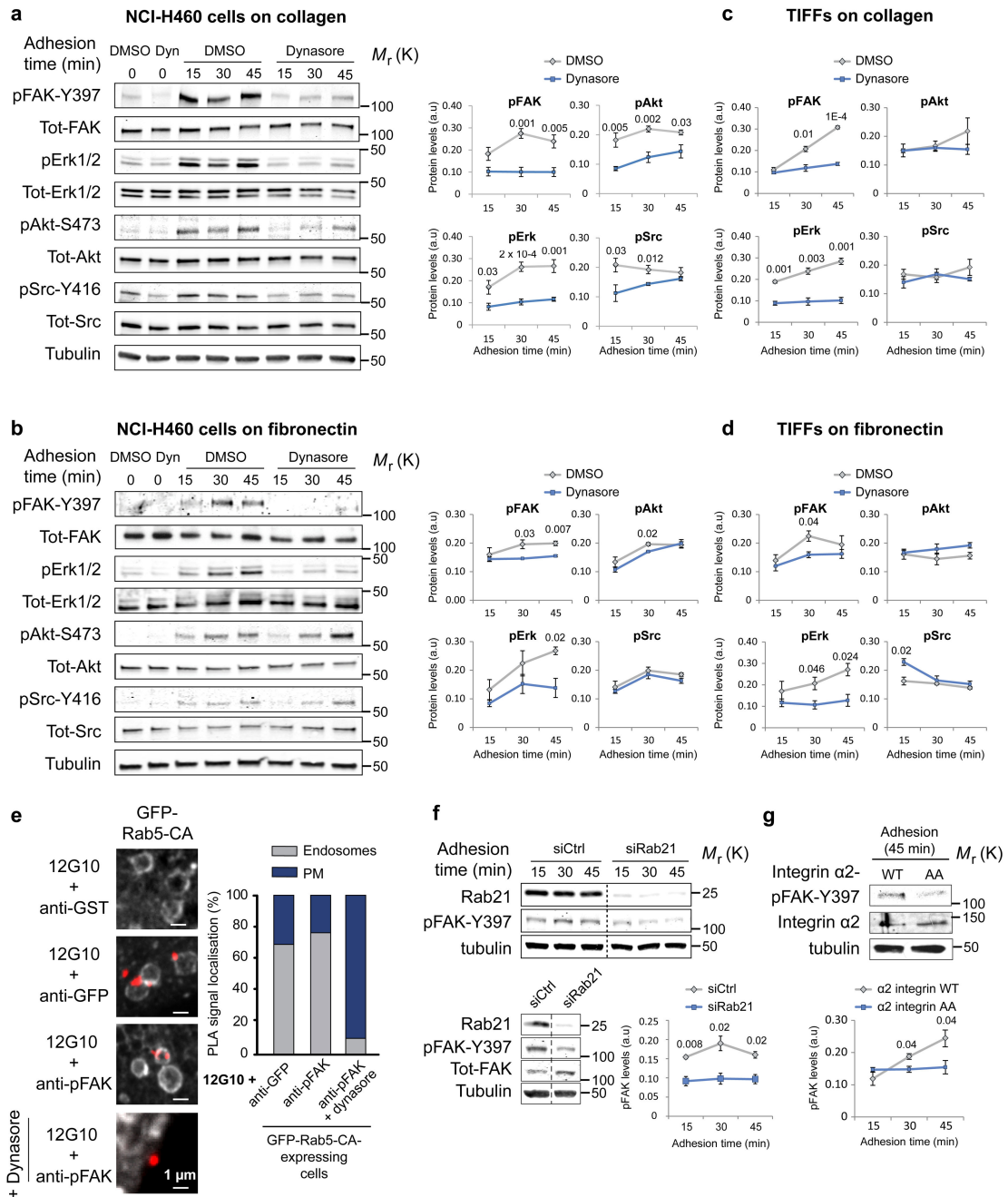


**Figure 3. Inhibition of integrin endocytosis attenuates integrin signalling.**

**a-d**, Analysis of kinase activity in NCI-H460 cells (**a, b**) and TIFFFs (**c, d**)  $\pm$  dynasore plated on collagen (**a, c**) or fibronectin (**b, d**) (mean  $\pm$  SEM, **a**,  $n=5$  independent experiments; **b-d**,  $n=3$  independent experiments). **e**, In-situ PLA signal (red dots) representing colocalisation between 12G10 (active integrin antibody) and the indicated antibodies in GFP-Rab5-CA-expressing cells (10 cells assessed from two independent experiments). **f**, Representative immunoblot and quantification of pFAK protein levels in Rab21- or control-silenced NCI-H460 cells plated on collagen for the indicated times (mean  $\pm$  SEM,  $n=3$  independent

experiments). **g**, Representative immunoblot and quantification of pFAK in CHO cells expressing  $\alpha 2$ -integrin wild-type (WT) or Rab21-binding deficient integrin  $\alpha 2$ -AA-mutant and plated on collagen for 45 min (mean  $\pm$  SEM, n=3 independent experiments). a.u: arbitrary units. Student's two-tailed unpaired t-test *P* values are provided and statistics source data can be found in Supplementary Table 2.

Uncropped images of blots are shown in supplementary figure 9.

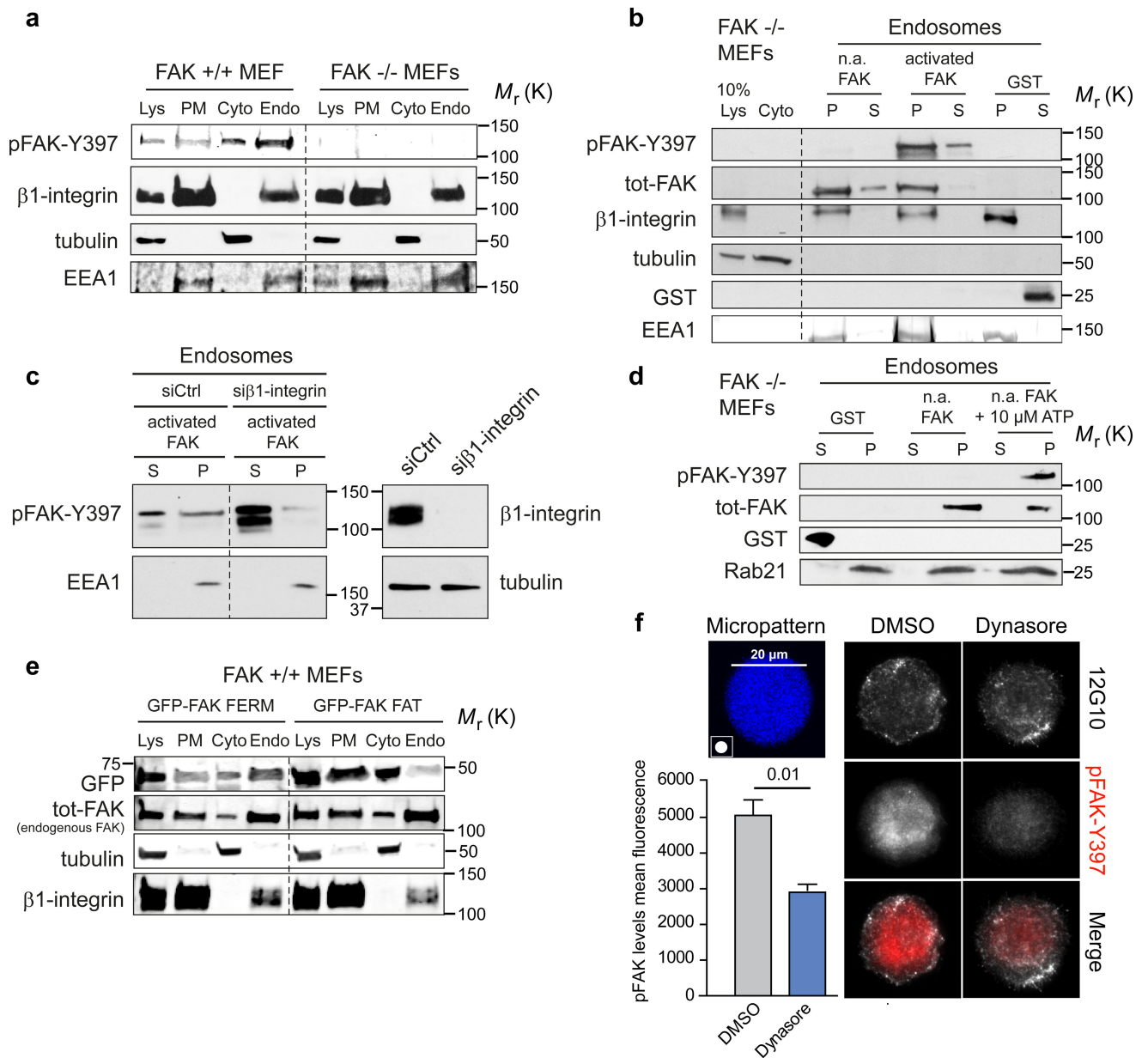


**Figure 4. FAK recruitment and activation on integrin-positive endosomes**

**a**, Representative immunoblot of subcellular fractionation of FAK<sup>+/+</sup> and FAK<sup>-/-</sup> MEFs (five independent experiments). **b**, Representative immunoblot of recombinant FAK (phosphorylated/activated or non-activated: n.a) recruitment to insoluble endosomal pellet (P) and soluble supernatant (S) fractions isolated from FAK<sup>-/-</sup> MEFs (five independent experiments). **c**, Representative immunoblot analysing the recruitment of recombinant FAK to purified endosomes derived from either control- or  $\beta$ 1-integrin-silenced FAK<sup>-/-</sup> MEFs (five independent experiments). **d**, Representative immunoblot analysing the activation of recombinant FAK in purified endosome fractions derived from FAK<sup>-/-</sup> MEFs in the presence or absence of 10  $\mu$ M ATP (five independent experiments). **e**, Subcellular fractionation of FAK<sup>+/+</sup> MEFs transfected with GFP-FAK FAT or GFP-FAK FERM. Shown

are representative immunoblots of GFP-FAK fragments and endogenous FAK (total-FAK) from two independent experiments. **f**, MDA-MB-231 cells plated on 20  $\mu\text{m}$  round fibronectin-coated micropatterns (45 min)  $\pm$  dynasore. Representative maximum projections and quantification of pFAK (mean fluorescence  $\pm$  SEM,  $n=3$  independent experiments, 10 cells analysed / experiment). Lys: cell lysate; PM: plasma membrane; Cyto: cytosol; Endo: Endosomal fraction. Student's two-tailed unpaired t-test  $P=0.01$ . Uncropped images of blots are shown in supplementary figure 9.

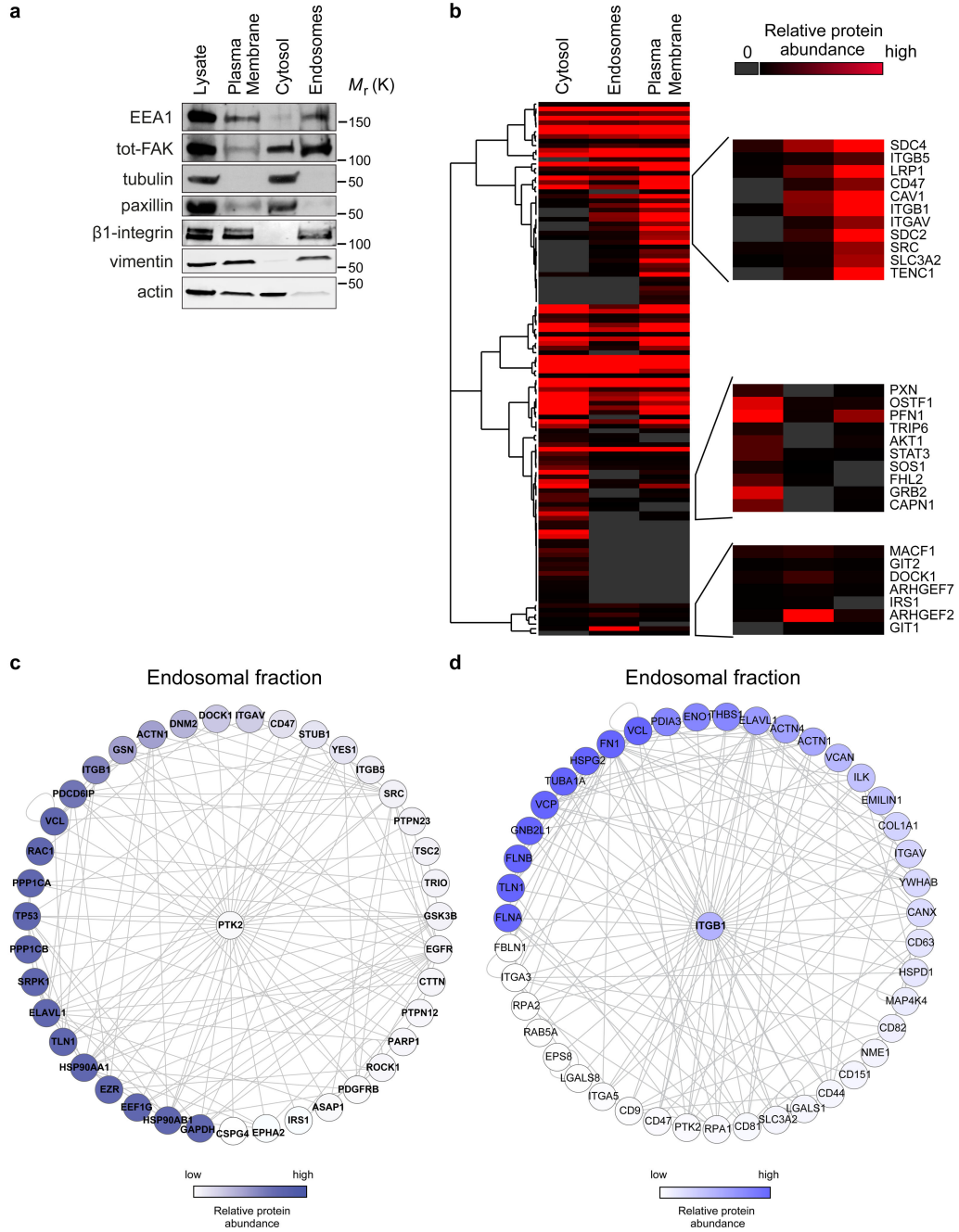


**Figure 5. Endosomal proteome.**

**a**, Representative western blot validation of fractionated samples analysed by mass spectrometry. **b-d**, The threshold for protein identification was set at a minimum of 3 spectral counts with at least 2 unique peptides. Altogether, 2021, 1667 and 2006 proteins were detected in the cytosolic, endosomal and plasma membrane fractions, respectively. **b**, Hierarchical clustering of Geiger adhesome proteins identified in the cytoplasmic, plasma membrane and endosomal fractions. Examples of proteins detected in multiple clusters are displayed on the right hand side (two independent experiments). **c-d**, Known FAK (PTK2)



(c) and  $\beta$ 1-integrin (ITGB1) (d) interacting proteins identified in the mass spectrometric analysis of purified endosomal fractions in FAK +/+ MEFs. Proteins were mapped onto a human protein-protein interaction network. Each node represents a protein (labelled with gene name) and each edge represents a reported interaction between two proteins. The nodes are coloured according to protein abundance (two independent experiments). Uncropped images of blots are shown in supplementary figure 9.

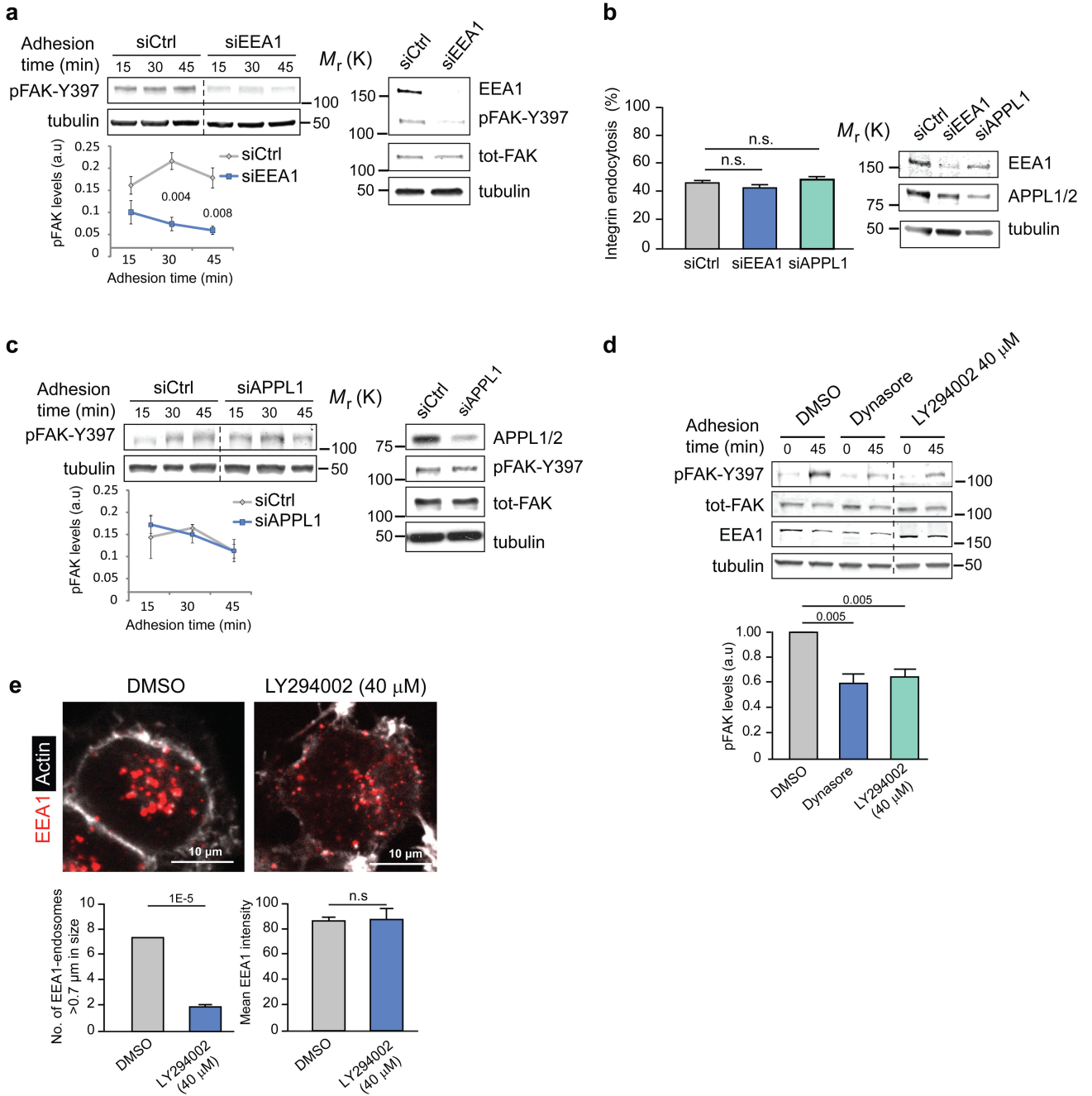


**Figure 6. Integrin signalling is EEA-1 dependent.**

**a, c,** Representative blots and quantification of pFAK protein levels following EEA1 (**a**) or APPL1 (**c**) silencing in NCI-H460 cells plated on collagen (mean  $\pm$  SEM, n=3 independent experiments). **b,** Integrin endocytosis in EEA1- or APPL1-silenced NCI-H460 cells plated on collagen (30 min) using active  $\beta$ 1-integrin (9EG7) antibody (proportion of cytoplasmic/total staining, mean  $\pm$  SEM, n=43 cells pooled from three independent experiments). **d,** Representative immunoblot and quantification of pFAK protein levels in NCI-H460 cells plated on collagen  $\pm$  dynasore or PI3K- inhibitor LY294002 (mean  $\pm$  SEM, n=3 independent

experiments). **e**, Representative confocal images of EEA1 and actin staining in NCI-H460 cells  $\pm$  PI3K inhibitor (LY294002 40  $\mu$ M) and quantification of the number of EEA1-endosomes larger than 0.7  $\mu$ m and the total mean EEA1 intensity (mean  $\pm$  SEM, n = 16 cells per condition pooled from two independent experiments). Student's two-tailed unpaired t-test *P* values are provided and statistics source data can be found in Supplementary Table 2. Uncropped images of blots are shown in Supplementary Figure 9.

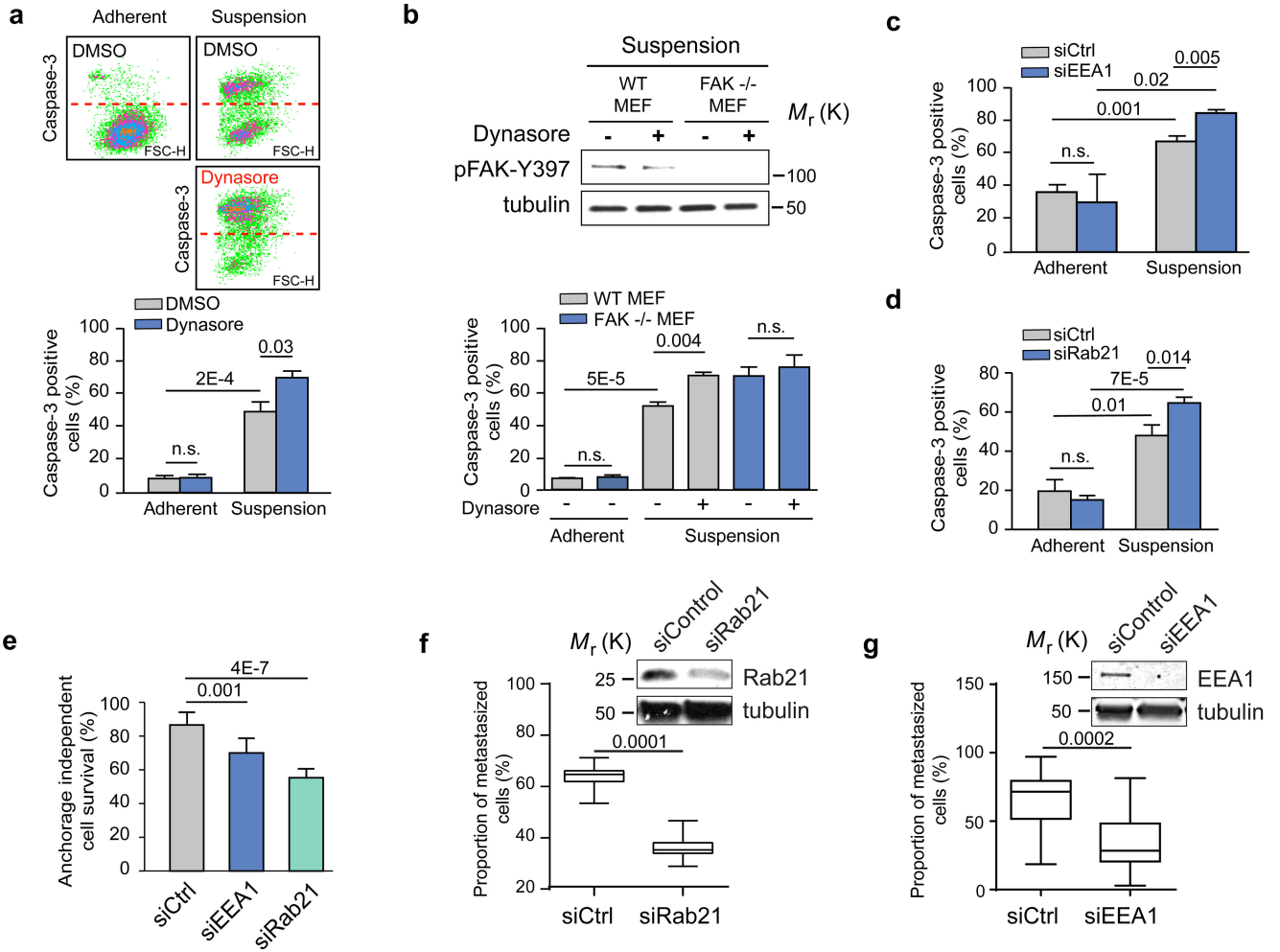


**Figure 7. Integrin endosomal signalling and anoikis sensitivity are Rab21- and EEA1-dependent.**

**a-d**, Quantification of caspase-3 positive (FL1) apoptotic cells in serum-starved TIFFs and representative dot blots (**a**), in FAK<sup>-/-</sup> or FAK<sup>+/+</sup> WT MEFs ± dynasore (**b**) and following EEA1 (**c**) or Rab21 (**d**) silencing in TIFFs (mean fluorescence ± SEM, n=3 independent experiments). **e**, Quantification of anchorage-independent survival of MDA-MB-231 cells following EEA1 or Rab21 silencing (mean ± s.d., n=3 independent experiments). **a-e**, Student's two-tailed unpaired t-test *P* values are provided. **f-g**, MDA-MB-231 cells transfected with siCtrl and siRab21 (**f**) or siCtrl and siEEA1 (**g**) were fluorescently labelled with green or far-red cell trackers and coinjected 1:1 into the tail vein of mice. The proportion of extravasated cells was analysed by flow cytometry 48 hr after coinjection and is represented as a percentage of total extravasated cells in the lung (box plots show the 25th–75th percentiles delineated by the upper and lower limits of the box; the median is shown by the horizontal line inside the box. Whiskers indicate maxima and minima; siRab21: n = 15 mice from one experiment, siEEA1: n=10 & 15 mice pooled from two independent experiments). Student's two-tailed unpaired t-test *P* values are provided.

Uncropped images of blots are shown in supplementary figure 9. Statistics source data can be found in Supplementary Table 2.

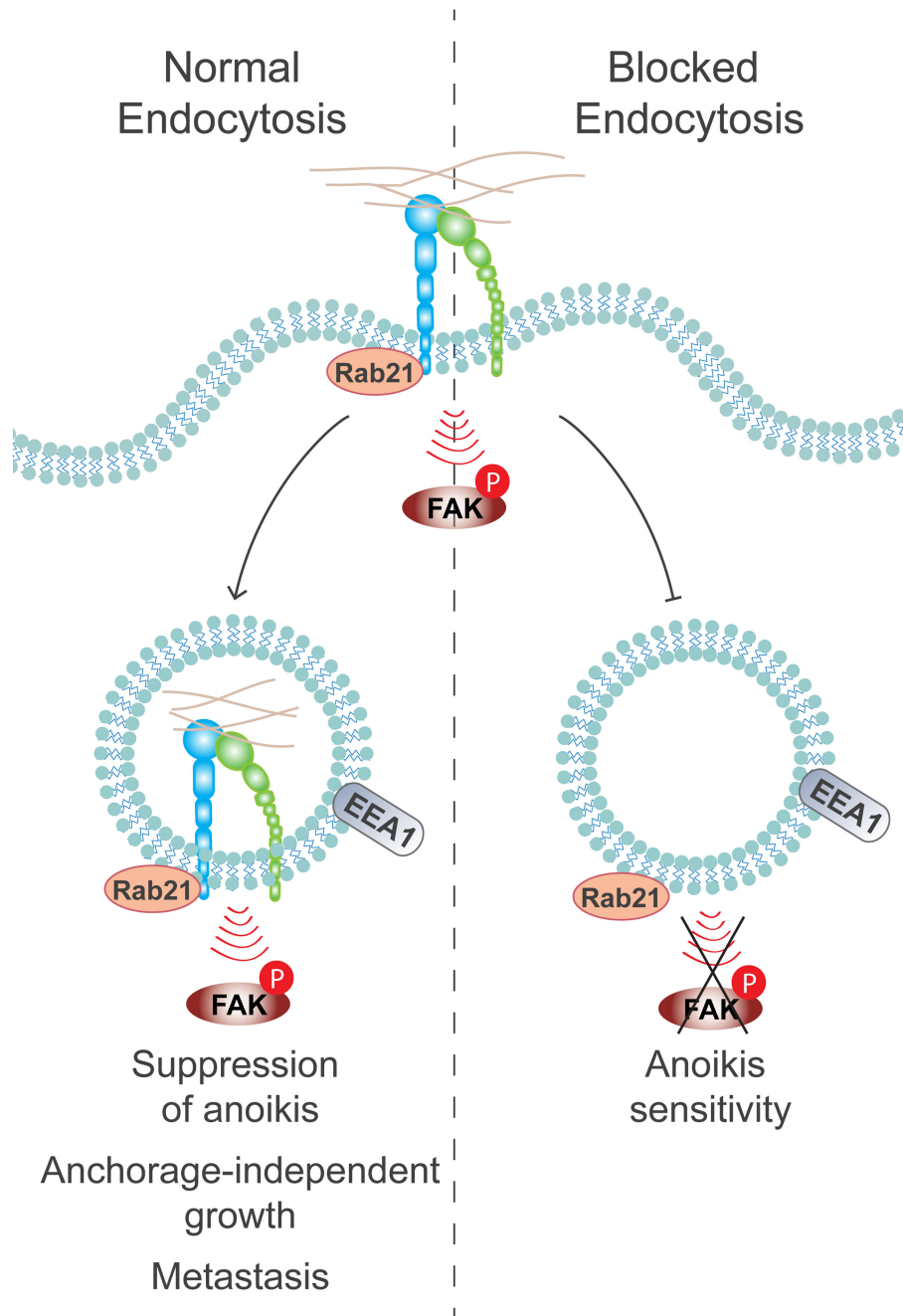


**Figure 8. Conclusion model: the role of adhesion-induced integrin endosomal signalling in the regulation of anoikis.**

The full activation of the ECM-induced integrin pFAK-Y397 signal is dependent on Rab21-mediated integrin endocytosis to EEA1-containing early endosomes, and this is ultimately required for suppression of anoikis and anchorage-independent growth. Blocked integrin endocytosis leads to reduced FAK activation and to increased anoikis sensitivity.